Supporting Information

Antibody-targeting of Ultra-small Nanoparticles Enhances Imaging Sensitivity and Enables Longitudinal Tracking of Multiple Myeloma

Alexandre Detappe[1,2,3,4], Mairead Reidy[1,2], Yingjie Yu[3], Clelia Mathieu[1,2], Hung V.-T. Nguyen[5], Thibaud P. Coroller[2,6], Fred Lam[3], Petr Jarolim[2,7], Peter Harvey[8], Andrea Protti[9], Quang-De Nguyen[9], Jeremiah A. Johnson[5], Yannick Cremilleux[10], Olivier Tillement[11], Irene M. Ghobrial[1,2,*], and P. Peter Ghoroghchian[1,2,3,*]

1. Department of Medical Oncology, Dana-Farber Cancer Institute, Boston MA 02215, U.S.A.
2. Harvard Medical School, 25 Shattuck Street, Boston MA 02115, U.S.A.
3. David H. Koch Institute for Integrative Cancer Research, Massachusetts Institute of Technology, Cambridge, Massachusetts 02139, U.S.A.
4. Centre Paul Strauss, 3 rue de la porte de l'hôpital, 67000 Strasbourg, France
5. Department of Chemistry, Massachusetts Institute of Technology, Cambridge, MA 02139, U.S.A.
6. Department of Radiation Oncology, Dana-Farber Cancer Institute, Boston MA 02215, U.S.A.
7. Department of Pathology, Brigham and Women's Hospital, Boston, Massachusetts 02115, USA
8. Department of Biological Engineering, Massachusetts Institute of Technology, Cambridge, Massachusetts 02139, U.S.A.
9. Lurie Family Imaging Center, Department of Radiology, Dana-Farber Cancer Institute and Harvard Medical School, Boston, MA, United States
10. Institut des Sciences Moléculaires, Université de Bordeaux, UMR CNRS 5255, 33076 Bordeaux
11. Institut Lumière Matière, UMR 5306 Université Lyon1-CNRS, Université de Lyon, 69622 Villeurbanne Cedex, France

*To whom correspondence should be addressed:

Irene M. Ghobrial, M.D.
Dana-Farber Cancer Institute,
450 Brookline Avenue,
Boston, MA 02215
Phone: 617-632-4198
email: Irene_Ghobrial@dfci.harvard.edu

P. Peter Ghoroghchian, M.D., Ph.D.
Koch Institute at MIT,
77 Massachusetts Avenue, 76-261F
Cambridge, MA 02139
Phone: (617) 715-4470
email: ppg@mit.edu

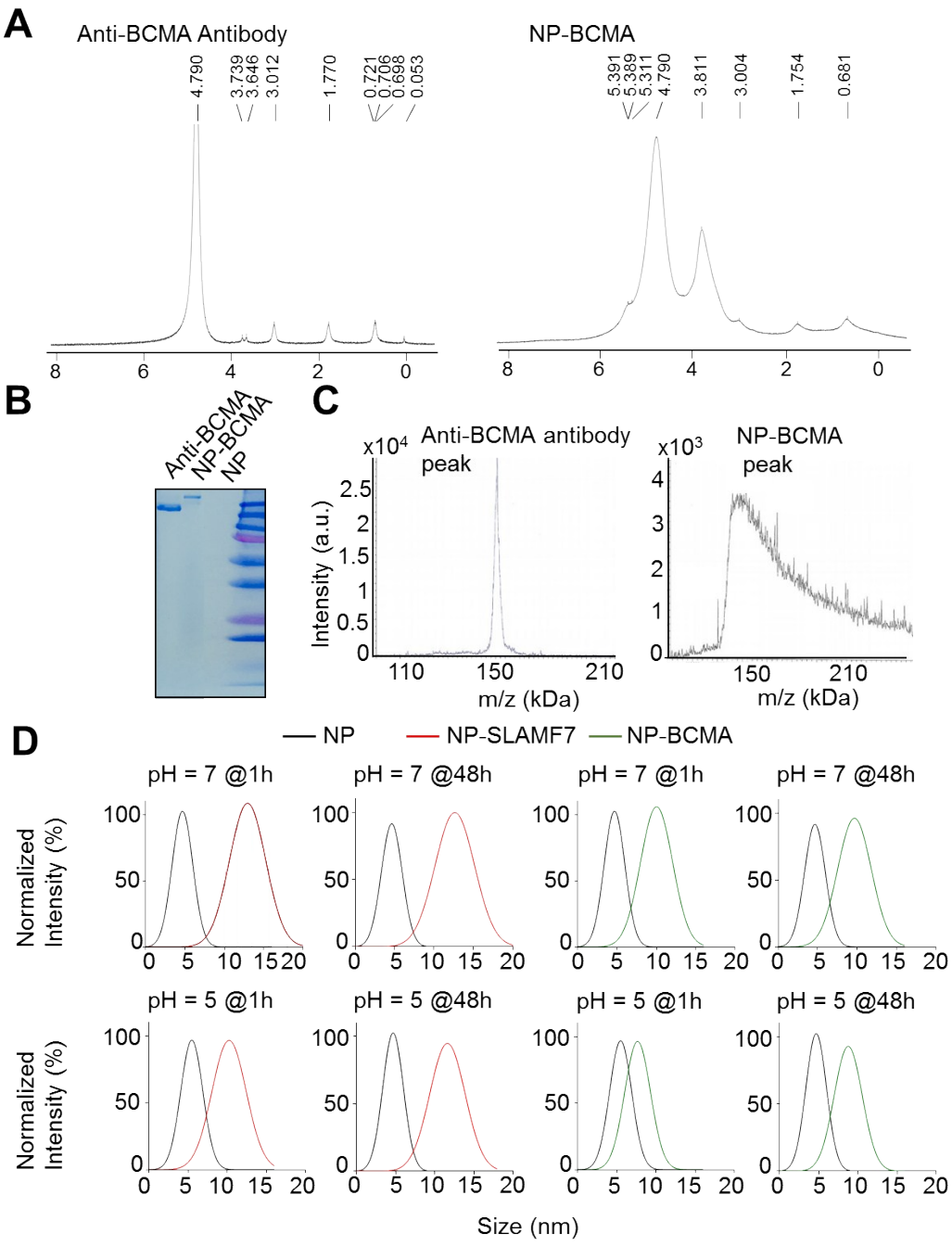

Supplementary Figure 1. Conjugation of gadolinium (Gd)-containing nanoparticles (NPs) to monoclonal antibodies. **A**. NMR traces confirming the presence of anti-BCMA antibodies before (left) and after conjugation to NPs (right) in purified suspensions. **B**. PACE experiment confirming the binding of anti-BCMA antibodies to NPs. **C.** MALDI-MS experiment validating the successful conjugation of the anti-BCMA antibody (left) to NPs, forming NP-BCMA (right). **D**. DLS measurements showing the stability of various NP-based suspensions before (blue) and after conjugation to either anti-SLAMF7 or anti-BCMA antibodies, generating NP-SLAMF7 (red) and NP-BCMA (green), respectively, over time and under different pH conditions.

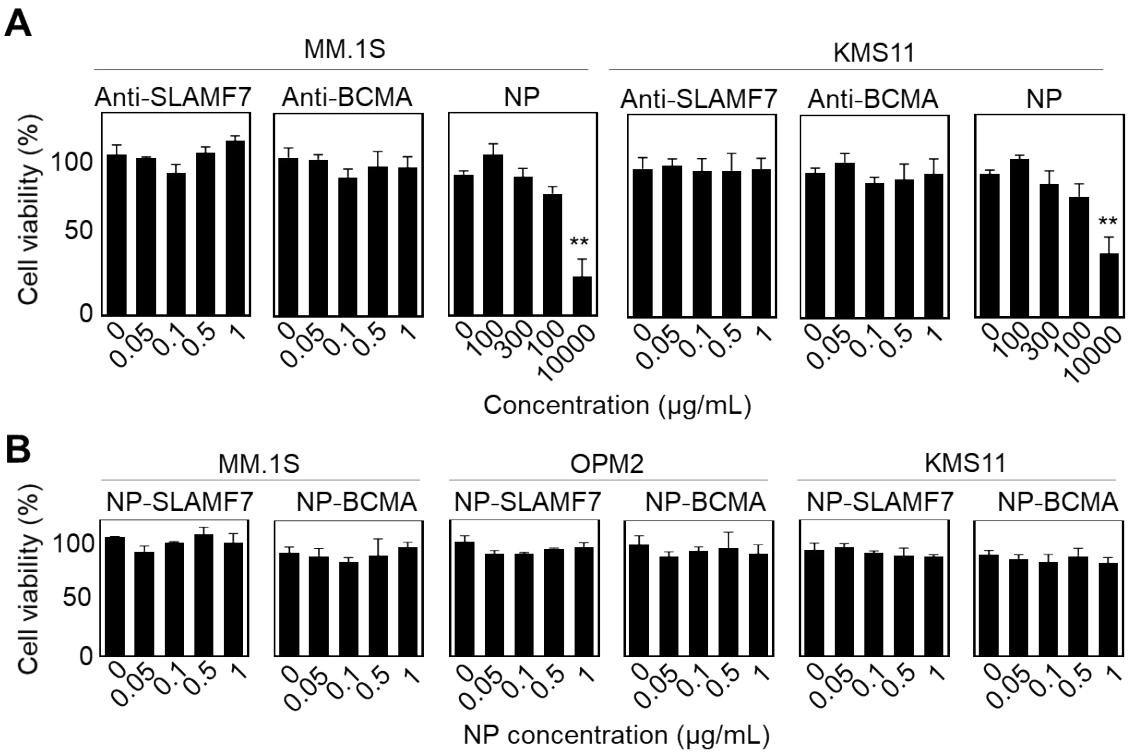

Supplementary Figure 2. Determination of the relative *in vitro* toxicity of NP-antibody complexes. A. Cellular viabilities of two different MM cell lines (MM.1S and KMS11) as determined via the CellTiter 96 Aqueous One Solution Proliferation Assay and as a function of incubation with increasing concentrations of 2 different monoclonal antibodies (anti-SLAMF7, anti-BCMA) or unmodified Gd-containing nanoparticles (NPs). **B**. Cellular viability as assessed after incubation of MM.1S, OPM2, and KMS11 cells with either of the formed NP-antibody complexes (*i.e.,* NP-SLAMF7 or NP-BCMA). All cellular viability measurements were conducted at 72 h after treatment addition; data are presented as the mean ± standard deviation for n=3 experimental replicates with each having n=5 technical replicates per condition. ** p-value<0.01, unpaired two-tailed t-test with Welch's correction.

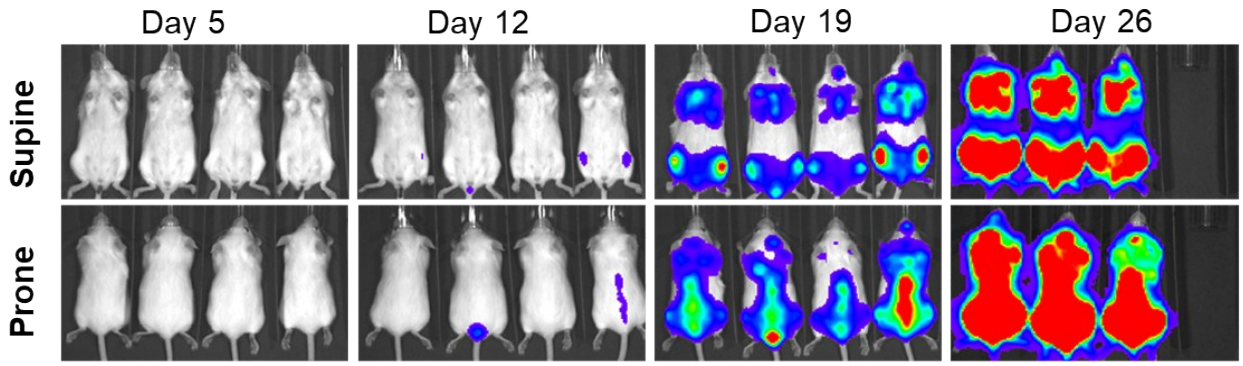

Supplementary Figure 3. Tracking the growth of plasmacytomas in an orthotopic cell-line xenograft model of multiple myeloma, using bioluminescence imaging (BLI). Human LUC^{+}-$MM.1S_{GFP}$ cells were introduced into 4 mice via IV dissemination and BLI was performed at various time points thereafter. For the MRI studies, the models were similarly established and imaging commenced on Day 19 after tumor cell implantation, which was first time point at which the tumor burden in the femurs and spines could be readily discerned via imaging.

A

	Antibody (mg/mL)	Gadolinium amount (µg)
Stock solution	0.50	100000.00
Coupling reaction	0.50	3124.47
1st purification	0.49	724.471
2nd purification	0.48	474.96
3rd purification	0.48	548.76
4th purification	0.48	568.20
5th purification	0.48	576.78
Final injectate suspension (administered in 200 µL per mouse)	0.096	548.76

B

	NP only	Unconjugated NP + anti-BCMA
	Gadolinium amount (µg)	Gadolinium amount (µg)
Stock solution	100000.00	100000.00
1st purification	97.46	211.13
2nd purification	4.11	33.97
3rd purification	0.03	3.21
4th purification	0.02	0.04

Supplementary Figure 4: Purification of ultra-small nanoparticle-antibody complexes by tangential filtration. A. Removal of free/unmodified NPs from suspensions of NP-BCMA. Congruent with the methods reported in prior publications[1-3], a 50 kDa cutoff membrane was used for tangential filtration to enable removal of unmodified NPs (~10 kDa) from suspension. Antibody concentrations were determined by the bicinchoninic acid assay and ICP-MS measurements were conducted to determine the Gd content that remained in solution upon subsequent rounds of tangential filtration (15,000 rcf, 50 kDa cutoff membrane). Note that this purification procedure could not nor was intended to remove free/unmodified anti-BCMA antibody (MW ~150 kDa); but, serial measurements evinced that no changes in Gd content were observed after three filtration steps, which were subsequently adopted when preparing purified samples of NP-BCMA. The final suspensions were concentrated prior to animal administration (200 µL/mouse) and each injectate contained 0.0956 mg (4.8 mg/kg) of antibody along with ~550 µg of Gd (~175 µmol/kg). **B.** Validation that only trace amounts of free/unmodified NPs remained in suspension after three rounds of tangential filtration. Unmodified NPs alone or upon mixture with free anti-BCMA antibodies were subjected to the same tangential filtration steps for purification as described in A. The results confirmed that only trace amounts of free/unmodified NPs remain after three rounds of purification and that the finale injectate suspensions contained only NP-BCMA and free anti-BCMA antibodies.

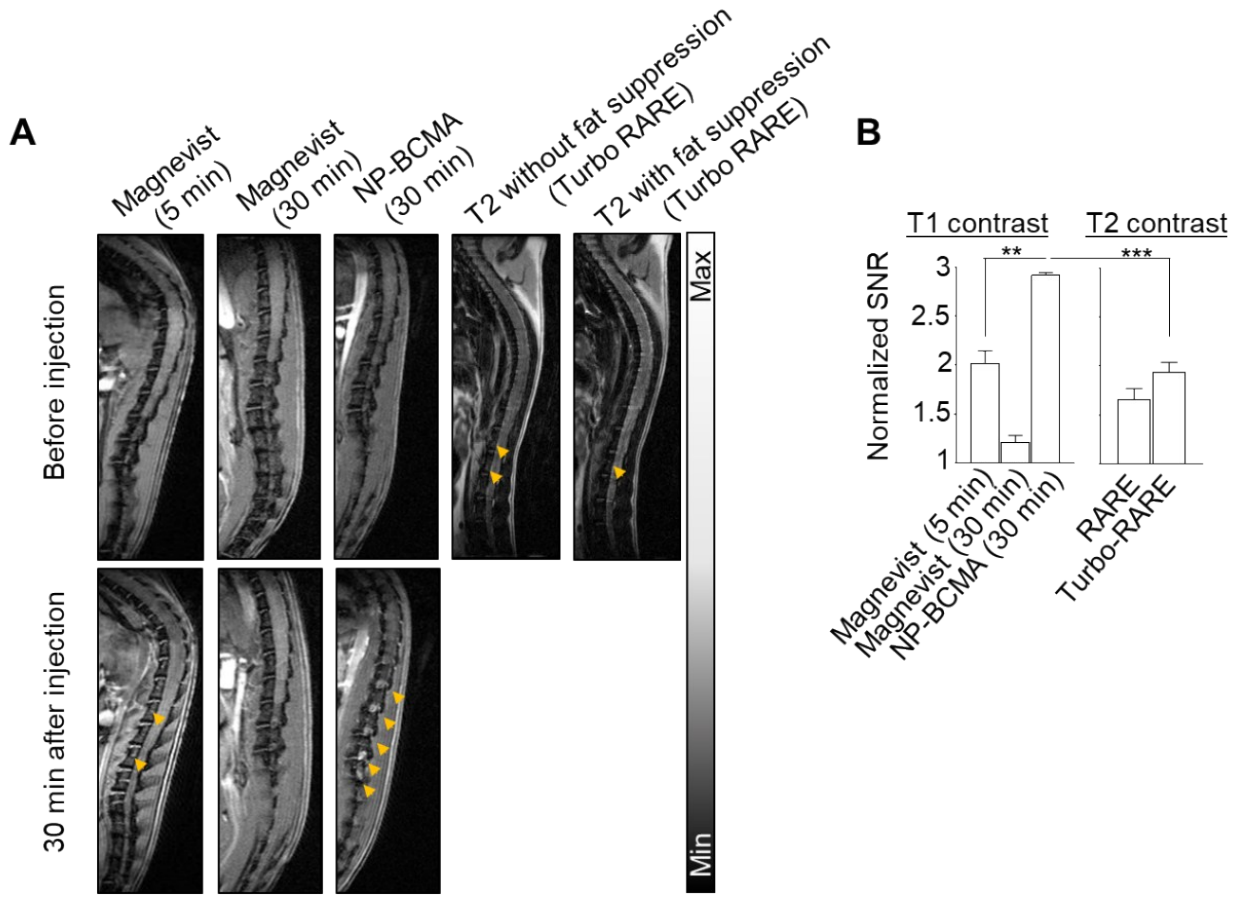

Supplementary Figure 5. Comparisons of imaging sensitivity achieved with various MR contrast agents and sequences. A. Qualitative representation of the signal enhancement for plasmacytomas (yellow arrows) and **B.** quantitative comparison of the signal-to-noise ratio (SNR) in the spines of MM.1S orthotopic tumor-bearing mice as determined by MRI at different time points after injection of T1-weighted contrast agents (i.e., Magnevist and NP-BCMA) as well as by employing various T2 sequences (n = 5 mice per group). Note the mice were administered the various contrast agents and/or imaged on day 19 after IV dissemination of LUC^{+}-$MM.1S_{GFP}$ cells. Statistical analyses were performed in order to compare the SNR of the T1 signal of NP-BCMA to that other contrast agents and/or alternative MRI sequences, ** p-value <0.01, ***p-value<0.001, two-tailed t-test. Pre-injection T2 weighted image: T2 turbo rare sequence with a repetition time of 3000 ms, echo time of 62.4 ms, ETL of 15 and 4 averages; the acquisition matrix = 192 x 192 pixels, the reconstructed matrix = 192 x 256 pixels, FOV of 24x40 mm, slice thickness = 0.5 mm; and, the sequence was performed with and without fat suppression. Post-injection T1 was based on the same protocol as the one described in the manuscript but with a shorter time interval between injection and imaging with Magnevist (i.e., 5 min).

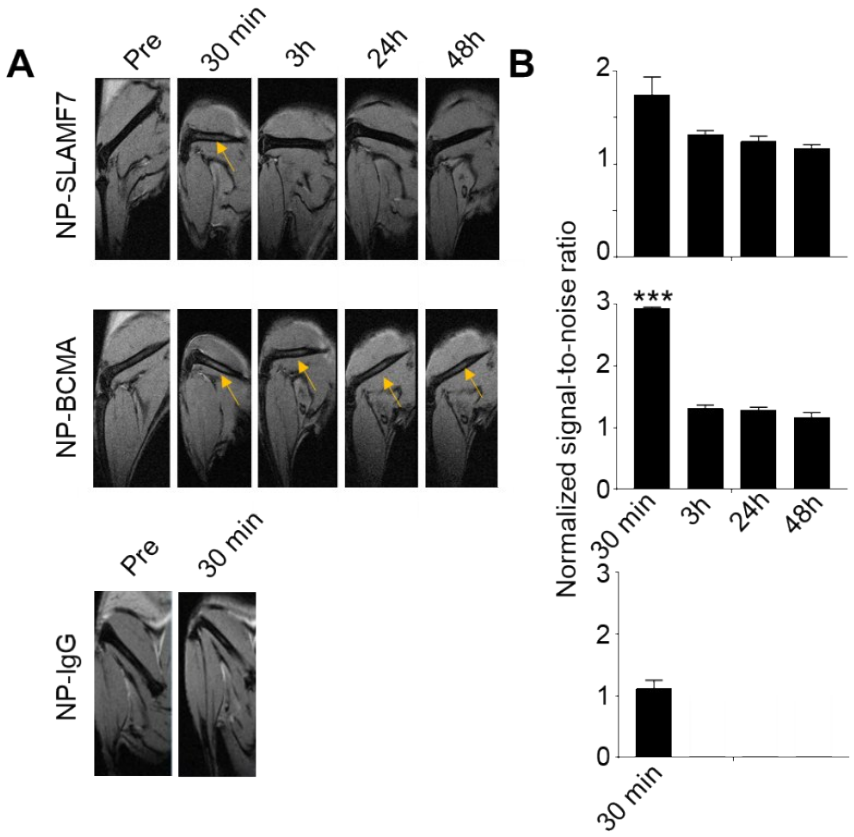

Supplementary Figure 6. Nanoparticle uptake in the femurs of MM1.S tumor-bearing mice on day 19 post- tumor-cell implantation. A. Representative MRI images obtained at designated time intervals after IV administration of NP-SLAMF7 (top), NP-BCMA (center), or NP-IgG (control; bottom). **B.** The signal-to-noise ratio (SNR) in the femurs of the animals were determined at each time point after injection of the various NP-antibody complexes (n = 5 mice/group; treatment groups correspond to the adjacent images found in the same row in part A). * p-values < 0.05, *** p-values<0.001, unpaired two-tailed t-test with Welch's correction.

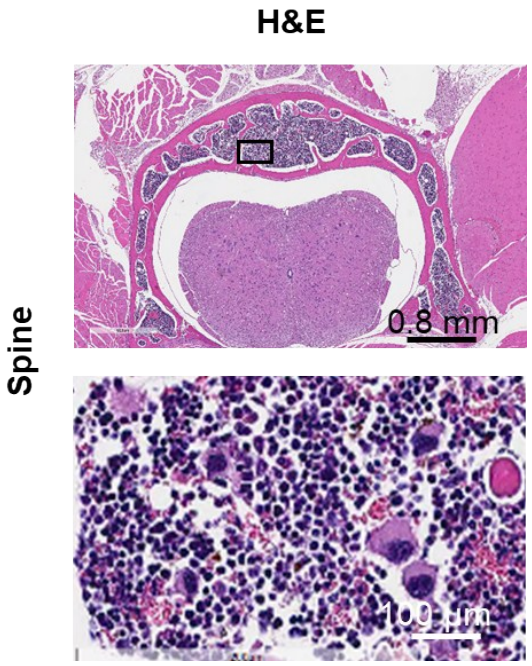

Supplementary Figure 7. Histological assessment of tumor burden after tissue sectioning and H&E staining of the spine of a mouse that was administered NP-BCMA.

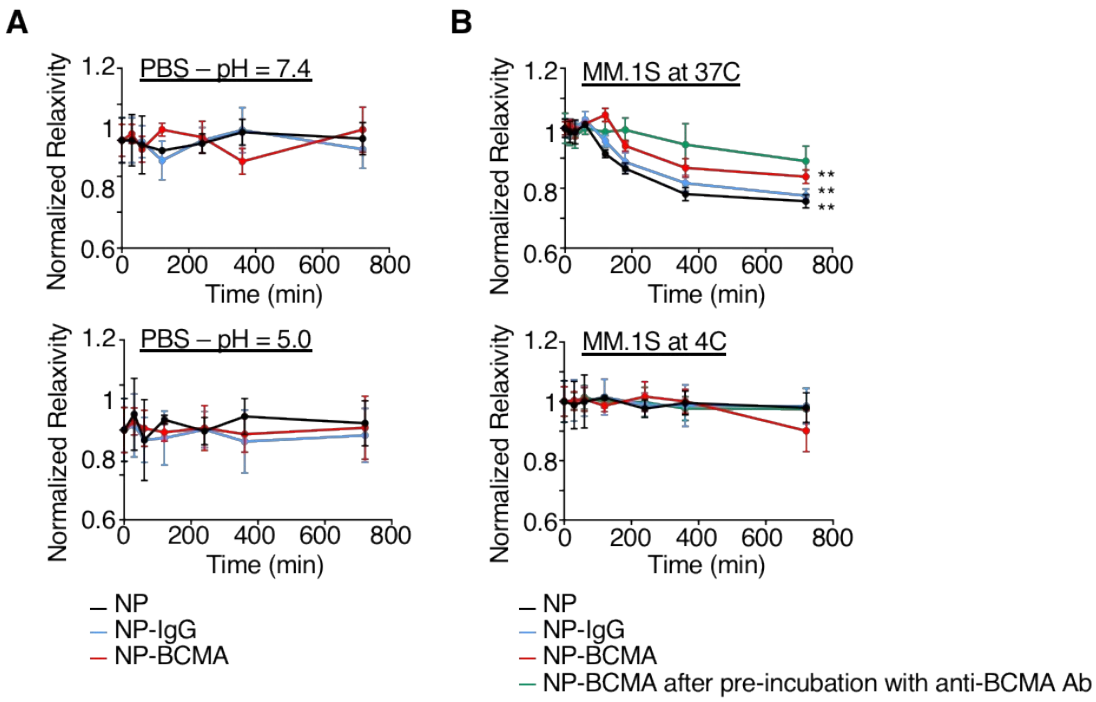

Supplementary Figure 8. Bioprocessing of nanoparticles post-tumor cell targeting results in a decrease in contrast enhancement. A. A stable r1 signal is observed from the unconjugated gadolinium-containing nanoparticle (NP) and from antibody-conjugated nanoparticles (i.e., NP-BCMA and NP-IgG) over time in both neutral and acidic pH solutions. **B**. After incubation with and internalization by MM.1S cells, bioprocessing of the nanoparticles leads to a decrease in their achievable relaxivity values. Incubation of the cells at 4 ^{o}C prior to nanoparticle addition prevents internalization, limiting subsequent nanoparticle bioprocessing and loss of signal enhancement. For this experiment, MM.1S cells (2,000 cells/well) were seeded in a 386-well plate overnight and treated with various nanoparticle-containing solutions (1 mM). The relaxivity measurements at various time points were compared to the value obtained for the nanoparticles at time zero; and, the experiment was repeated in triplicate. The reported values represent the mean +/- standard deviation. A Kruskall-Wallis test was performed to compare the relaxivity change between t = 0 min and t = 720 min., ** p-value < 0.01.

A

NP	Mouse 1	Mouse 2	Mouse 3	Mouse 4	Mouse 5	Average
(1) Average dose (μmol Gd/kg mouse)						**183.97**
(2) Average weight of mouse (kg)						**0.02**
(3) Average spine weight (g)						**0.90**
(4) Gd3+ in whole spine as determined by ICP-MS (μg)	1.44	0.49	0.37	0.26	0.35	**0.58**
(5) Gd3+ dose level in whole spine (μmol/kg) = (4)/[157.25*(3)*0.001]	10.17	3.48	2.59	1.82	2.49	**4.11**
(6) %ID/g in whole spine = 100*(5)/[(1)*(2)*1000]	0.27	0.09	0.07	0.05	0.07	**0.11**

B

NP-SLAMF7	Mouse 1	Mouse 2	Mouse 3	Mouse 4	Mouse 5	Average
(1) Average dose (μmol Gd/kg mouse)						**174.37**
(2) Average weight of mouse (kg)						**0.02**
(3) Average spine weight (g)						**0.90**
(4) Gd3+ in whole spine as determined by ICP-MS (μg)	14.18	11.33	6.89	7.12	7.06	**9.32**
(5) Gd3+ dose level in whole spine (μmol/kg) = (4)/[157.25*(3)*0.001]	100.18	80.03	48.71	50.30	49.89	**65.82**
(6) %ID/g in whole spine = 100*(5)/[(1)*(2)*1000]	2.87	2.29	1.40	1.44	1.43	**1.89**

C

NP-BCMA	Mouse 1	Mouse 2	Mouse 3	Mouse 4	Mouse 5	Average
(1) Average dose (μmol Gd/kg mouse)						**174.49**
(2) Average weight of mouse (kg)						**0.02**
(3) Average spine weight (g)						**0.90**
(4) Gd3+ in whole spine as determined by ICP-MS (μg)	21.04	25.33	24.09	16.03	22.16	**21.73**
(5) Gd3+ dose level in whole spine (μmol/kg) = (4)/[157.25*(3)*0.001]	148.66	178.98	170.22	113.26	156.58	**153.54**
(6) %ID/g in whole spine = 100*(5)/[(1)*(2)*1000]	4.26	5.13	4.88	3.24	4.49	**4.40**

Supplementary Figure 9. Quantitative determination of Gd uptake in the spines of animals at 30 min after systemic (IV tail-vein) administration of A. NP, B. NP-SLAMF7 and C. NP-BCMA. An average Gd level of 153.54 ± 25.42 μmol/kg was calculated in the spines of animals treated with NP-BCMA, which equates to a 37-fold enhancement in the local Gd concentration in the spine when compared to untargeted NP, which is a vascular pooling agent that rapidly washes out of the bone marrow. Moreover, NP-BCMA exhibits a 2.3-fold enhancement in the local Gd concentration in the spine when compared to NP-SLAMF7. Together, these results demonstrate the capabilities of the antibody-targeted constructs (i.e., NP-BCMA and NP-SLAMF7) to bind to resident plasma cells in the spine; the increased accumulation of NP-BCMA supports the mechanism underlying its enhanced contrast enhancement as seen by MRI (Figs. 2C and S5) and may be attributed to the greater numbers of BCMA molecules on the surfaces of malignant plasma cells.

A

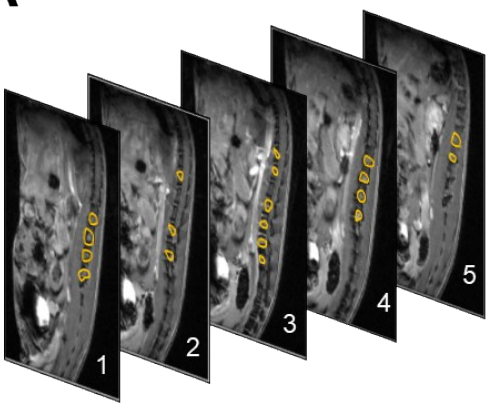

B

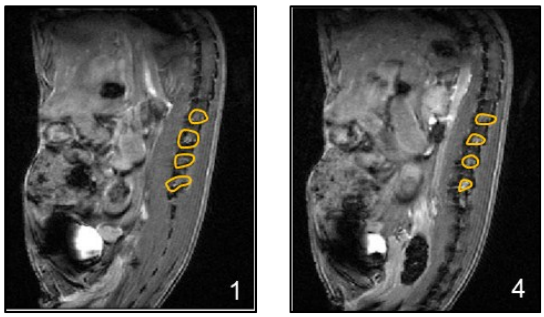

C

	Mouse 1	Mouse 2	Mouse 3	Mouse 4	Mouse 5	**Average**
Tumor area (mm^2 in 1 mm slice) = ∑(slide1-n)⟦tumor pixels⟧	16.35	24.6	28.6	19.9	16.8	**21.25**
Total spinal area (mm^2 in 1 mm slice) = ∑(slide1-n)⟦spine pixels⟧	240.08	332.43	407.99	341.34	243.83	**313.14**
%Spine comprised of tumor = 100*(Tumor Area)/(Total spinal area)	6.81	7.40	7.01	5.83	6.90	**6.79**

Supplementary Figure 10: Determination of the average tumor burden in the spines of MM.1S tumor-bearing mice on day 19 after tumor-cell implantation and as determined by MRI at 30 min after systemic (IV tail-vein) injection of NP-BCMA. A. Tumor sites segmented for an n=5 mice that were similarly processed, using ImageJ software. **B.** Representative segmented images of the spines of two separate mice (#1 and #4), corresponding to those in part A, where plasmacytomas (yellow) are visualized based on the T1 signal enhancement afforded by NP-BCMA. **C.** Total tumor and spinal areas as well as the % of the spine comprised of tumor as determined by the summation of the total tumor and spinal areas in each segmented image for an n=5 mice that were similarly processed. The total tumor burden in the spine was found to comprise 6.79 ± 0.58 % of the spinal volume at the acquisition time (i.e., 19 days after tumor cell implantation).

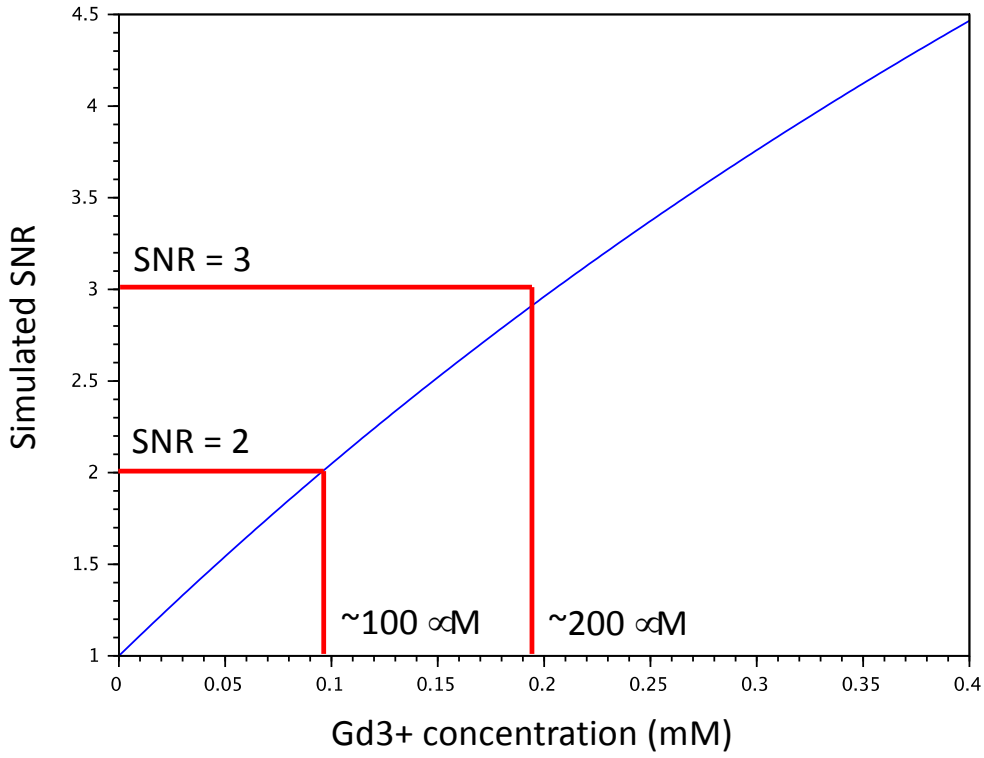

Supplementary Figure 11. Simulated signal-to-noise ratio as a function of Gd concentration. The normalized SNR that may be expected as a function of the local concentration of NPs was computed based on the T1 GRE sequence, where the NMR signal intensity (SI) = A.exp(-TE/T2*).sin(FA).(1-exp(-TR/T1))/(1-cos(FA).exp(-TR/T1)); note, A is a constant depending on the experimental conditions (i.e., number of detected nuclear spins, coil sensitivity, magnet field, spectrometer), TE is the MRI sequence echo time, T2* is the apparent transverse relaxation time, FA is the flip angle, TR is the MRI sequence repetition time, and T1 is the longitudinal relaxation time. A and the noise level are expected to remain constant between each image acquisition for a given animal. Similarly, exp(-TE/T2*) is assumed not to vary following NP administration, which otherwise changes the T1 value as follows: $1/T1 = 1/T1_o + r1.C$; note, r1 is the relaxivity of the NP ($mM^{-1}. S^{-1}$), C is the NP concentration (mM) and $T1_o$ is the T1 value before NP administration. Finally, the normalized SNR is equal to the ratio of (1-exp(-TR/T1))/(1-cos(FA).exp(-TR/T1)) over (1-exp(-TR/$T1_o$))/(1-cos(FA).exp(-TR/$T1_o$)). In determining the associations between SNR and the expected concentrations of Gd, the following values were used in the calculation of the normalized SNR: TR = 87 ms, FA = 60°, $T1_o$ = 2000 ms and r1 = 4.8 $mM^{-1}.s^{-1}$ per Gd^{3+} for NPs. Note that SNRs of 2 and of 3 were observed in the spines of MM.1S-tumor bearing mice on day 19 after cell inoculation and at 30 min after the administration of NP-SLAMF7 and NP-BCMA, respectively (**Figs. 2C** and **S5**), supporting that these targeted constructs are able to achieve local Gd concentrations between 100-200 μM as a result of specific targeting of resident plasmacytomas.

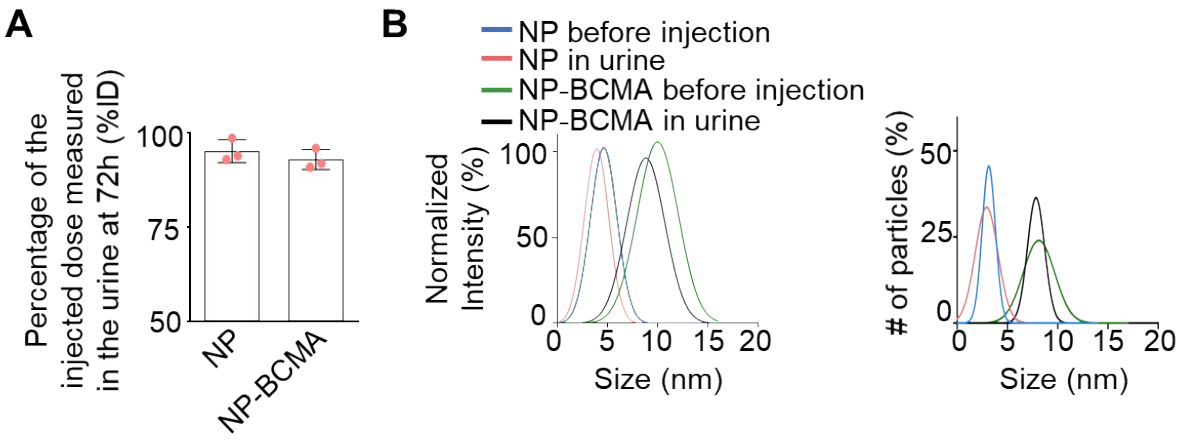

Supplementary Figure 12. Assessment of the extent of renal clearance and changes in nanoparticle size after intravenous injection. A. Nearly complete renal elimination of NP and NP-BCMA as observed at 72 h after systemic administration. **B.** Normalized intensity- (left) and number-weighted size distributions (right) of NP and NP-BCMA before intravenous administration and after isolation upon systemic clearance into the urine as determined by DLS.

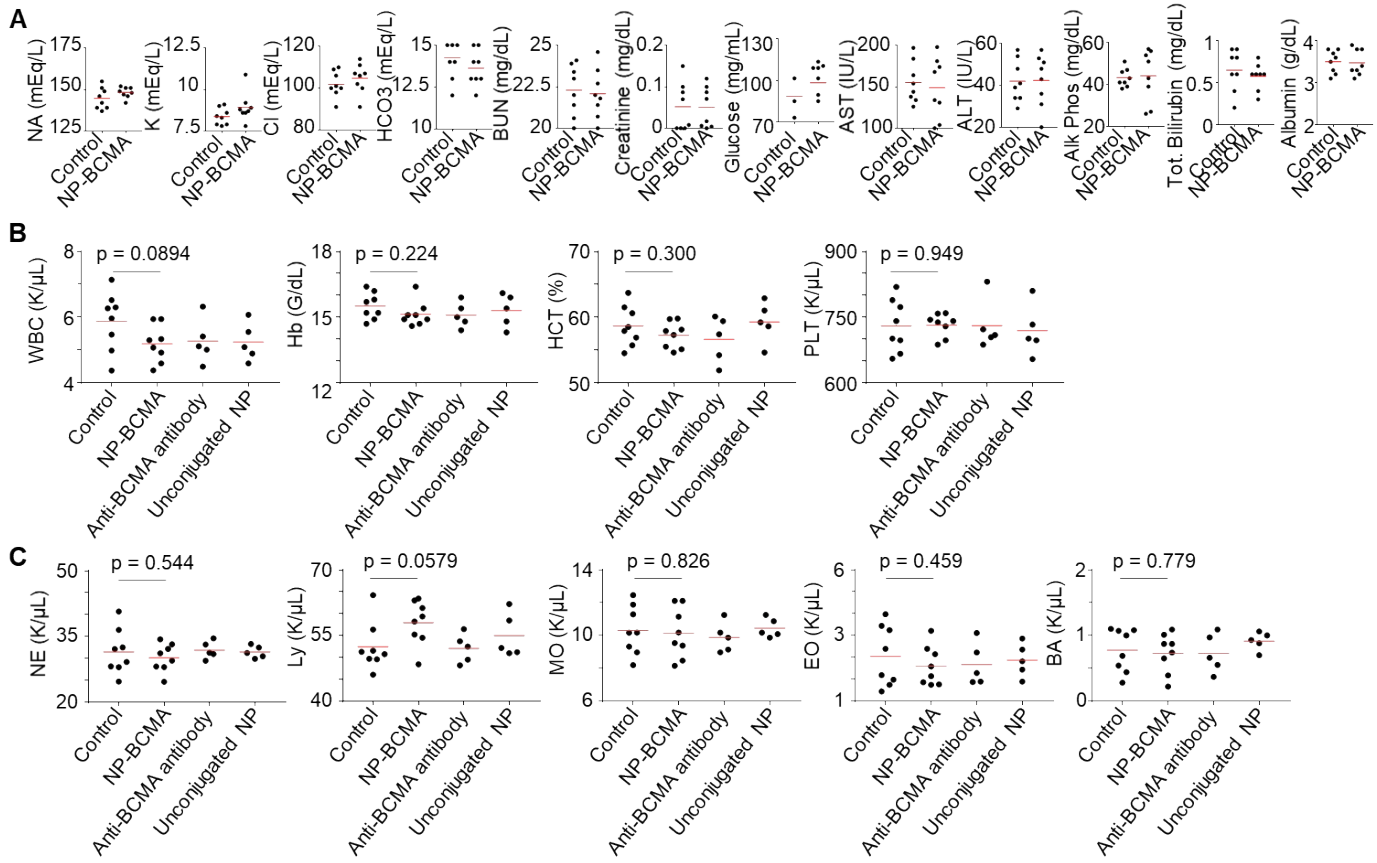

Supplementary Figure 13. **Preliminary toxicity evaluation of Gd-containing nanoparticles and their antibody complexes. A**. Basic metabolic profiles (n=8 mice per group), **B**. Complete blood counts, and **C**. white blood cell differential counts from healthy balb/c mice as assessed at 12 days after systemic administration of PBS (control; n = 8 mice), NP-BCMA (n = 8 mice), anti-BCMA antibody (n = 5 mice), or unconjugated NP (n = 5 mice). The unpaired two-tail t-test with Welch's correction was used to assess the statistical differences between the PBS (control) and NP-BCMA groups.

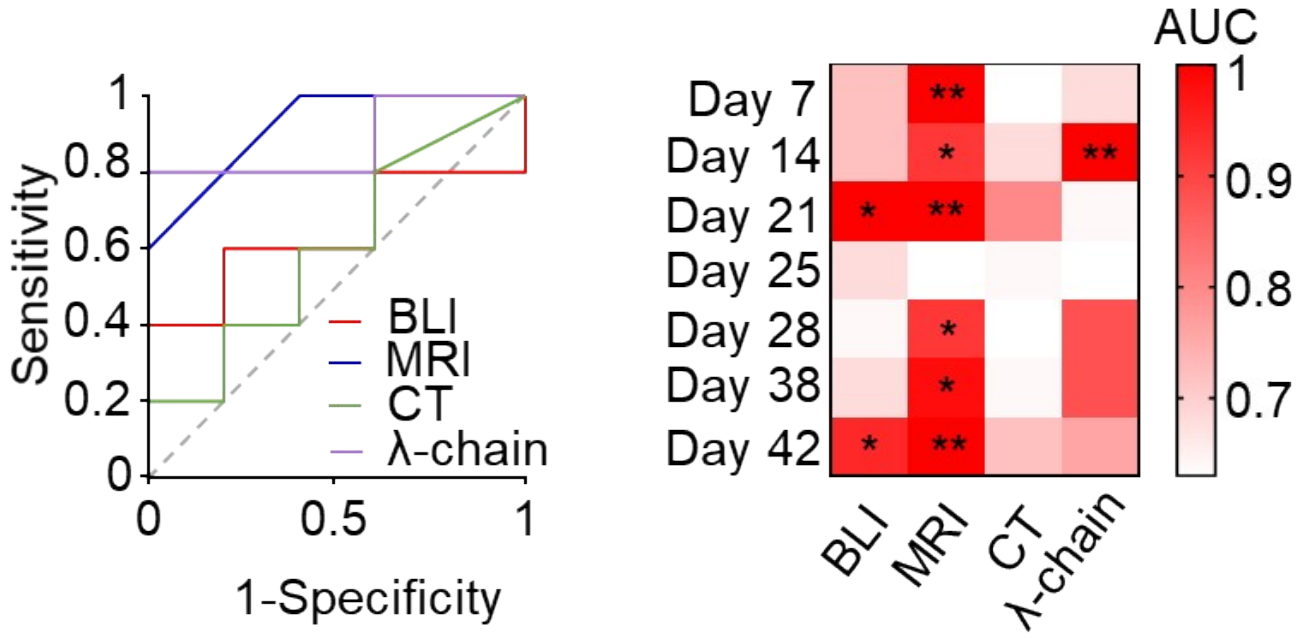

Supplementary Figure 14. Receiving operator chain curves (left) comparing the sensitivity and specificity of each diagnostic modality to assess the presence of tumor cells in mice. Analysis of the area under the curve (AUC) for each modality (right) as well as the statistical difference assessed by two-sided Wilcoxon rank-sum test. * p-value < 0.05, ** p<0.01.

References

1. Mignot, A.; Truillet, C.; Lux, F.; Sancey, L.; Louis, C.; Denat, F.; Boschetti, F.; Bocher, L.; Gloter, A.; Stephan, O.; Antoine, R.; Dugourd, P.; Luneau, D.; Novitchi, G.; Figueiredo, L. C.; de Morais, P. C.; Bonneviot, L.; Albela, B.; Ribot, F.; Van Lokeren, L.; Dechamps-Olivier, I.; Chuburu, F.; Lemercier, G.; Villiers, C.; Marche, P. N.; Le Duc, G.; Roux, S.; Tillement, O.; Perriat, P., A top-down synthesis route to ultrasmall multifunctional Gd-based silica nanoparticles for theranostic applications. *Chemistry* **2013,** *19* (19), 6122-36.

2. Lux, F.; Tran, V. L.; Thomas, E.; Dufort, S.; Rossetti, F.; Martini, M.; Truillet, C.; Doussineau, T.; Bort, G.; Denat, F.; Boschetti, F.; Angelovski, G.; Detappe, A.; Cremillieux, Y.; Mignet, N.; Doan, B. T.; Larrat, B.; Meriaux, S.; Barbier, E.; Roux, S.; Fries, P.; Muller, A.; Abadjian, M. C.; Anderson, C.; Canet-Soulas, E.; Bouziotis, P.; Barberi-Heyob, M.; Frochot, C.; Verry, C.; Balosso, J.; Evans, M.; Sidi-Boumedine, J.; Janier, M.; Butterworth, K.; McMahon, S.; Prise, K.; Aloy, M. T.; Ardail, D.; Rodriguez-Lafrasse, C.; Porcel, E.; Lacombe, S.; Berbeco, R.; Allouch, A.; Perfettini, J. L.; Chargari, C.; Deutsch, E.; Le Duc, G.; Tillement, O., AGuIX((R)) from bench to bedside-Transfer of an ultrasmall theranostic gadolinium-based nanoparticle to clinical medicine. *Br J Radiol* **2018**, 20180365.

3. Bouziotis, P.; Stellas, D.; Thomas, E.; Truillet, C.; Tsoukalas, C.; Lux, F.; Tsotakos, T.; Xanthopoulos, S.; Paravatou-Petsotas, M.; Gaitanis, A.; Moulopoulos, L. A.; Koutoulidis, V.; Anagnostopoulos, C. D.; Tillement, O., (68)Ga-radiolabeled AGuIX nanoparticles as dual-modality imaging agents for PET/MRI-guided radiation therapy. *Nanomedicine (Lond)* **2017,** *12* (13), 1561-1574.